THE JOURNAL OF BIOLOGICAL CHEMISTRY VOL. 286, NO. 16, pp. 14419–14426, April 22, 2011

Different Sequences Show Similar Quaternary Interaction Stabilities in Prohead Viral RNA Self-assembly*[S]

Received for publication, October 3, 2010, and in revised form, February 22, 2011 Published, JBC Papers in Press, February 24, 2011, DOI 10.1074/jbc.M110.191064

Xiaobo Gu and Susan J. Schroeder[1]

From the Departments of Chemistry and Biochemistry and Botany and Microbiology, University of Oklahoma, Norman, Oklahoma 73019

Prohead RNA (pRNA) is an essential component of the self-assembling ϕ29 bacteriophage DNA packaging motor. Different related species of bacteriophage share only 12% similarity in pRNA sequences. The secondary structure for pRNA is conserved, however. In this study, we present evidence for self-assembly in different pRNA sequences and new measurements of the energetics for the quaternary interactions in pRNA dimers and trimers. The energetics for self-assembly in different pRNA sequences are similar despite very different sequences in the loop-loop interactions. The architecture surrounding the interlocking loops contributes to the stability of the pRNA quaternary interactions, and sequence variation outside the interlocking loops may counterbalance the changes in the loop sequences. Thus, the evolutionary divergence of pRNA sequences maintains not only conservation of function and secondary structure but also stabilities of quaternary interactions. The self-assembly of pRNA can be fine-tuned with variations in magnesium chloride, sodium chloride, temperature, and concentration. The ability to control pRNA self-assembly holds promise for the development of nanoparticle therapeutic applications for this biological molecule. The pRNA system is well suited for future studies to further understand the energetics of RNA tertiary and quaternary interactions, which can provide insight into larger biological assemblies such as viruses and biomolecular motors.

Prohead RNA (pRNA)[2] is an essential component of the biomolecular motor that packages DNA into ϕ29 bacteriophage viral capsids (1, 2). At least four very different RNA sequences with conserved secondary structures (Fig. 1) (3) are capable of fulfilling this unique function in bacteriophage. The ϕ29 RNA interacts with the gp16 ATPase that drives the biological motor (4). Mutations in the pRNA can inactivate the biological motor and packaging activity (4–10). The role of pRNA and the mechanism of this biological motor are a controversial area of active research (11–15). This biological nanomotor can package the 19,300 bases of the ϕ29 DNA genome into the viral capsid against a load as high as 57 piconewtons with a maximum force exceeding 100 piconewtons, thus filling the capsid to >50% capacity and reaching internal pressures as high as 60 atm (16–19). Cryo-electron microscopy of *in vitro* assembled packaging motors showed a ring of five pRNAs interacting with a ring of five gp16 ATPases and a ring of 12 gp10 connector proteins to form the core of the nanomotor (12). Biophysical studies of the components of this motor can contribute to understanding how the motor assembles and works to package DNA.

pRNA is a natural sequence with the unique property of forming ring nanostructures. pRNA self-assembles in dimers, trimers, pentamers, and hexamers through loop-loop interactions (Fig. 2) (5, 9, 14, 15, 20). HNN-COSY NMR experiments have shown the formation of intermolecular hydrogen bonding in Watson-Crick pairs between two RNA hairpin models of the loop-loop interaction (21). All of the natural sequences for pRNA contain the potential for Watson-Crick pairing within the interlocking loops, *i.e.* the CE and D loops (Figs. 1 and 2). The novel self-assembly properties of pRNA are the basis for using pRNA as a nanoparticle building block and therapeutic delivery vector (22–29). RNA has a tremendous capacity for forming diverse nanostructures, including tRNA squares (30, 31), cubes (32), polyhedrons (33), nanorings (34), filaments (35), paranemic motifs (36), and nanocrowns (37). Understanding the sequence variation of pRNA self-assembly will enable future design of nanoparticles and nanomotors. This work provides the biophysical foundations for further studies on the structures and applications of this naturally self-assembling RNA nanoparticle.

Although previous studies have thoroughly explored the self-assembly of the ϕ29 RNA sequence (5, 9, 14, 15, 20, 38–40), biophysical studies on other pRNA sequences have not been pursued. The potential to form loop-loop interactions occurs in a very different surrounding architecture in the different natural pRNA sequences. The sequences of the multibranch and bulge loops vary, and the lengths of the helices that position the nucleotides to pair in the interlocking loops are very different in different pRNA sequences. This study reports the self-assembly of the M2, SF5, and GA1 pRNAs; the free energies for dimer formation; the effects of swapping interlocking loop sequences; and the differential effects of metal ions and temperature on pRNA multimerization. The self-assembly in the native pRNA sequences shows similar stabilities of dimer formation, although swapping the interlocking loop sequences results in different dimer stabilities. Evidently, sequence variation out-

* This work was supported in part by Grant HR09-160 from the Oklahoma Center for the Advancement of Science and Technology and by Institutional Research Grant 090039 from the American Chemical Society (to the University of Oklahoma Cancer Center).

[S] The on-line version of this article (available at http://www.jbc.org) contains supplemental Figs. S1–S10 and Tables S1–S3.

[1] Supported by National Science Foundation CAREER Grant 0844913. To whom correspondence should be addressed: University of Oklahoma, 101 Stephenson Pkwy., Norman, OK 73019. Tel.: 405-325-3092; Fax: 405-325-6111; E-mail: susan.schroeder@ou.edu.

[2] The abbreviation used is: pRNA, prohead RNA.

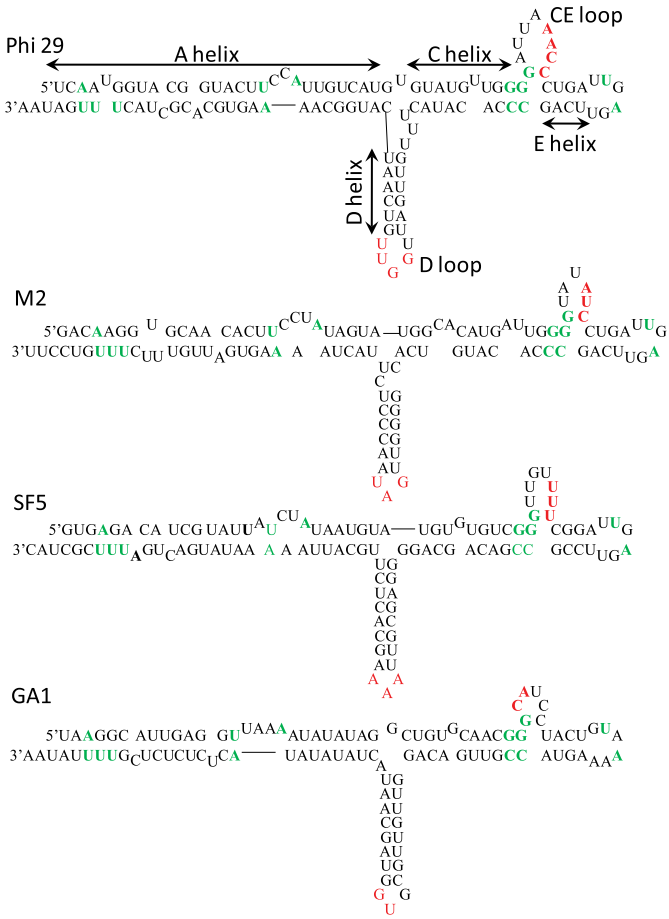

FIGURE 1. **Secondary structures of ϕ29, M2, SF5, and GA1 pRNAs.** Conserved nucleotides are *green*. Nucleotides that participate in potential Watson-Crick intermolecular tertiary and quaternary interactions between the CE bulge loop and the D loop hairpin are in *red*. The secondary structures shown were determined experimentally by enzymatic and chemical modification data (3). Three additional pRNA sequences have also been proposed from phylogenetic alignments (9).

side the interlocking loops may compensate for the different stabilities of loop-loop interactions. Thus, the divergent pRNA sequences maintain not only secondary structure and function but also the energetics of quaternary interactions.

EXPERIMENTAL PROCEDURES

RNA Preparation—The sequences of M2 and GA1 pRNAs were cloned from genomic DNA provided by Dr. Shelley Grimes (University of Minnesota). A synthesized DNA sequence (Integrated DNA Technologies) was used as template for SF5 sequence amplification. The PCR product was ligated into the pGEM-T vector (Promega Corp.). A plasmid for the ϕ29 pRNA sequence was kindly provided by Dr. Nicola Stonehouse (University of Leeds). Loop mutants were prepared by site-specific PCR mutation of plasmid pGEM-T pRNA using a Stratagene QuikChange kit. The primers used in this study are listed in supplemental Tables S1 and S2. The identity of all clones was confirmed by the DNA sequencing facility at the University of California at Davis. The RNAs were produced by T7 *in vitro* transcription (41) and purified by denaturing PAGE. pRNA was ^{32}P-labeled using T4 polynucleotide kinase, and the purity was >90%. The RNA was dialyzed at least three times

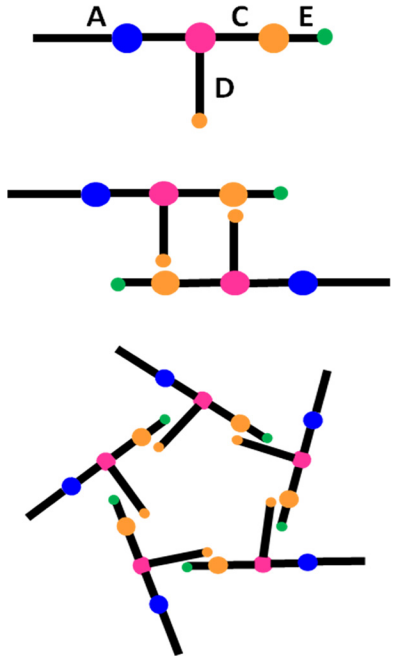

FIGURE 2. **Ball-and-stick model of pRNA monomer, dimer, and pentamer.** Loops are represented as *balls*, and helices are represented as *sticks*. The angles between helices are shown as right angles for simplicity, but coaxial stacking and helix orientations have not been experimentally determined yet. The helices are labeled in the monomer diagram. Helix B extends from the 3′-end of helix A in the full-length 174-mer pRNA but is not necessary for self-assembly or motor function and is not shown. The CE bulge loop and the D hairpin loop are shown as *orange balls*. Base pairing interactions between the CE and D loops is proposed to occur in pRNA dimers and multimers. The arrangement of pRNA in a pentamer is based on cryo-electron microscopy of *in vitro* assembled packaging motors (12).

using Centricon filters to equilibrate the RNA in defined salt and buffer conditions.

Sedimentation Velocity Analysis—Analytical ultracentrifugation experiments were conducted in the same buffer conditions as used for native gels to determine the molecular weight of gel bands. Sedimentation velocity experiments were run at 4 °C and 35,000 rpm in a Beckman XLA centrifuge with an An-60 TI rotor. The rotor and cells were pre-equilibrated at 4 °C, and the samples were renatured from 90 to 4 °C by snap cooling on ice. The buffer for the sample was 90 mM Tris, 200 mM boric acid, 5 mM NaCl, and 10 mM $MgCl_2$ (pH 7.5). Standard double sector cells were loaded with 500 μl of buffer and 500 μl of the appropriate sample solution. Absorbance scans at a wavelength of 260 nm were acquired at 10-min intervals. Buffer density and viscosity were calculated to be 1.0064 g/ml and 1.0871 poise at 4 °C, respectively. A value of 0.55 ml/g was used for the partial specific volume for the RNAs (14, 15). Data were analyzed with UltraScan-9.9 software and fit using van Holde-Weischet analysis, two-dimensional spectrum analysis, and genetic algorithm analysis (42, 43).

Native Gel Electrophoresis—Detailed renaturing protocols for each gel with specific buffers are included in the figure legends. After at least 30 min of equilibration, the pRNA sample was mixed with 40% (w/v) sucrose loading buffer and run on a 10% polyacrylamide gel buffered at pH 7.5 in 90 mM Tris and 200 mM boric acid with different concentrations of NaCl or $MgCl_2$. The gel and buffer were precooled for 4 °C experiments. Gels were exposed to a PhosphorImager screen and read with a

TABLE 1

Molecular weight distribution of ϕ29, M2, SF5, GA1, and mutant 1 pRNAs in analytical ultracentrifugation

The pRNA samples are renatured from 90 to 4 °C by snap cooling on ice in 5 mM NaCl and 10 mM $MgCl_2$ with 90 mM Tris and 200 mM boric acid (pH 7.5). The reported molecular weights in grams/mol are from the genetic algorithm analysis with an estimated error of 10% from all sources of experimental error. The molecular weights of species 1 are consistent with monomer molecular weights. The molecular weights of species 2 are consistent with a dimer conformation. —, no conformation was observed with this molecular weight.

pRNA	Concentration[a]	Species 1 M_r	Population	Species 2 M_r	Population	Higher order species	Population
		g/mol × 10^4	%	*g/mol* × 10^4	%	*g/mol* × 10^4	%
ϕf29	High	—	—	8.62 ± 0.86	76.3	11.28 ± 1.13	23.7
ϕ29	Low	3.31 ± 0.33	11.6	7.34 ± 0.73	70.1	11.95 ± 1.20	18.3
M2	High	4.25 ± 0.43	12.2	8.13 ± 0.81	43.9	11.21 ± 1.12	44.0
M2	Low	3.94 ± 0.39	22.7	8.34 ± 0.83	77.3	—	—
GA1	High	3.70 ± 0.37	82.8	7.95 ± 0.80	17.2	—	—
GA1	Low	4.21 ± 0.42	100	—	—	—	—
SF5	High	3.54 ± 0.35	2.2	6.25 ± 0.63	24.5	13.63 ± 1.36	73.2
SF5	Low	3.90 ± 0.39	28.8	6.95 ± 0.70	19.2	13.72 ± 1.37	52.0
Mutant 1[b]	High	4.42 ± 0.44	100	—	—	—	—
Mutant 1[b]	Low	4.09 ± 0.41	100	—	—	—	—

[a] The low and high concentrations are 0.3 A_{260} and 0.8 A_{260}. The extinction coefficients of ϕ29, M2, GA1, SF5, and mutant 1 pRNAs are 1,168,000, 1,203,400, 1,192,900, 1,178,000, and 1,152,900 (51).

[b] Mutant 1 is a pRNA sequence with only U nucleotides in the interlocking loops.

GE Storm scanner. Band intensities were quantified with ImageQuant software. The molecular weights for conformations of ϕ29, M2, GA1, and SF5 at high and low concentrations were determined by analytical ultracentrifugation to accurately identify monomer and dimer bands. DNA ladders were used only as control markers for consistency in running many native gels.

For measurements of dissociation constants of the native pRNA sequences, the same amount of ^{32}P-labeled pRNA was added to serial dilutions of unlabeled pRNA over an ~1000-fold concentration range. The concentration of monomer was calculated from the ratios of the band intensities and then plotted as monomer concentration *versus* fraction multimer (supplemental Fig. S1). The slope of the line indicates the equilibrium constant between monomer and dimer formation, according to the following equations for dimer and trimer formation, respectively: 2 pRNA ↔ $pRNA_2$, $[mono] = K_{d2}([total]/[mono] - 1)/2$; and 3 pRNA ↔ $pRNA_3$, $[mono]^2 = K_{d3}([total]/[mono] - 1)/3$, where [mono] is the concentration of pRNA in the monomer state, and [total] is the total pRNA concentration. The reported dissociation constants for the conditions shown in Fig. 3 are the average of at least three measurements with an estimated error of ±15%. The dissociation constants for natural pRNAs in other conditions and mutant pRNA sequences were estimated from the results presented in Fig. 4 and supplemental data.

UV Optical Melting—UV absorbance was measured with a Beckman DU800 spectrometer equipped with a temperature controller. Absorbance *versus* temperature curves of the pRNA were measured at 260 nm in 100 mM NaCl and 10 mM sodium cacodylate (pH 7.0) containing various concentrations of $MgCl_2$. The heating rate was 1 °C/min. Before melting, the pRNA sample was renatured from 90 to 4 °C by snap cooling on ice.

Circular Dichroism Spectroscopy—The CD spectra of pRNA sequences at 4 °C were measured for 3 μM pRNA using a J-820 spectropolarimeter (JASCO Co., Ltd., Hachioji, Japan) with a 0.1-cm path length quartz cell. The CD spectrum was obtained by taking the average of three scans made at 0.5-nm intervals from 200 to 400 nm. Before measurement, the pRNA sample was renatured from 90 to 4 °C by snap cooling on ice. The temperature of the cell holder was regulated by a PTC-348 temperature controller (JASCO Co., Ltd.), and the cuvette-holding chamber was flushed with a constant stream of dry N_2 gas to avoid water condensation on the cuvette.

RESULTS AND DISCUSSION

All Natural pRNA Sequences Form Monomers, Dimers, and Higher Order Multimers—Table 1 shows the molecular weights of pRNA conformations measured at low and high concentrations of pRNA. Analytical ultracentrifugation separates different conformations on the basis of mass, size, and shape. For ϕ29, M2, GA1, and SF5, the first species had a molecular weight consistent with a monomer pRNA, and the second species had a molecular weight consistent with dimer formation. The percentage of the population in the dimer conformation increased at higher pRNA concentrations. Accurate analysis became more difficult for more than two species and at higher molecular weights; however, the next species appeared to be consistent with trimer formation. The SF5 pRNA sequence showed many higher order species. The pRNA sequence with only U nucleotides in the interlocking loops, mutant 1, formed only one conformation with a molecular weight consistent with monomer formation. The analytical ultracentrifugation experiments identified monomer and dimer conformations of ϕ29, M2, GA1, and SF5, providing benchmarks for native gel experiments.

Dissociation Constants for Different pRNA Sequences Are Similar Despite Different Interlocking Loop Sequences—Fig. 3 shows the native gel analysis of natural pRNA sequences forming dimers and trimers. At low concentrations, M2 and GA1 pRNA sequences formed only monomers and dimers (Fig. 3 and supplemental Fig. S2). These lanes were thus used to calculate the equilibrium constant for dimer formation. At very low concentrations, SF5 formed a monomer and trimer. Then as the concentration increased, more SF5 monomer formed dimer and trimer and higher order multimers. Thus, a simple dissociation constant for SF5 dimerization could not be calculated. Instead, the low SF5 concentration lanes were used to calculate the equilibrium constant for trimer formation. An estimate of the SF5 dimerization dissociation constant could be

calculated with the assumption that dimer formation is not an intermediate in trimer formation.

The ϕ29 sequence showed a sharper transition from monomer to dimer in the absence of sodium chloride (Fig. 3*B*), which is the best ionic condition for the calculation of ϕ29 dimerization dissociation constants. The measured dissociation constant for ϕ29 dimerization is 6.45×10^{-7} M in the presence of 10 mM $MgCl_2$, which agrees within experimental error with previous measurements made by equilibrium sedimentation (44). M2 and GA1 also formed dimers in 10 mM $MgCl_2$ (supplemental Figs. S3 and S4). Each natural sequence responded slightly differently to changes in ionic conditions, which can complicate direct comparisons of energetics measurements. However, in 10 mM $MgCl_2$ with or without 5 mM NaCl, the dissociation constants are within experimental error for the calculation of free energies.

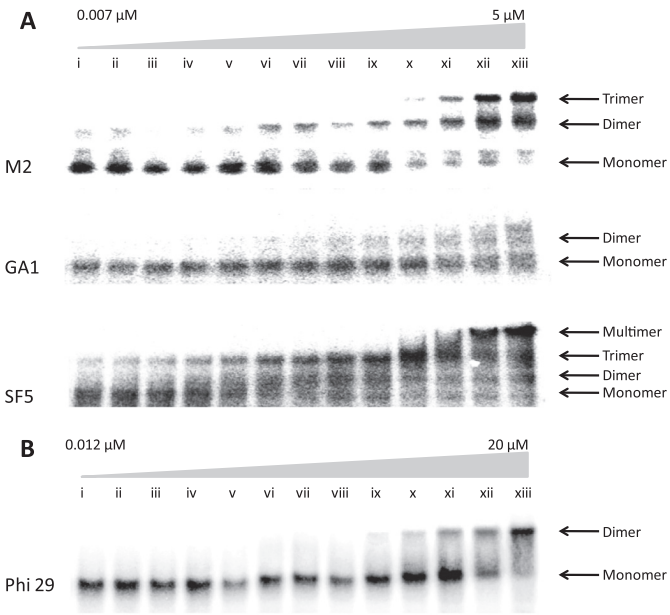

FIGURE 3. **M2, GA1, SF5, and ϕ29 pRNA self-assembly in serial dilutions.** *A*, the pRNA concentrations in *lanes i–xiii* are 0.007, 0.009, 0.01, 0.02, 0.03, 0.05, 0.1, 0.2, 0.3, 0.6, 1.3, 2.5, and 5 μM, respectively. The pRNA samples were renatured from 90 to 4 °C by snap cooling on ice in 5 mM NaCl and 10 mM $MgCl_2$ with 90 mM Tris and 200 mM boric acid (pH 7.5). The native polyacrylamide gel was run at 4 °C with the same buffer conditions as the pRNA sample. *B*, the ϕ29 pRNA samples were renatured from 90 to 4 °C by snap cooling on ice in 10 mM $MgCl_2$ with 90 mM Tris and 200 mM boric acid (pH 7.5). The pRNA concentrations in *lanes i–xiii* are 0.012, 0.022, 0.032, 0.051, 0.090, 0.17, 0.33, 0.64, 1.3, 2.5, 5.0, 10, and 20 μM, respectively. The gels were analyzed with ImageQuant software, and background correction values were <10%. Additional bands in the same lanes outside of the region of gel shown were not observed. The positions of monomer and dimer bands were benchmarked using analytical ultracentrifugation experiments. DNA size markers were used only as a reference for consistency in comparing many different gels (supplemental Table S3). Additional gel data at different pRNA concentrations and ionic conditions are included in supplemental Figs. S2–S6.

The dissociation constants and free energies for pRNA self-assembly are summarized in Table 2. All four natural pRNA interlocking loop sequences contain possible Watson-Crick pairing. The predicted free energies for the Watson-Crick pairing between loops were calculated using the INN-HB model and Turner rules (45). If Watson-Crick pairing were the only contribution to the stability of pRNA self-assembly, then a range of 5 orders of magnitude in dissociation constants would be predicted for pRNA self-assembly. In contrast, the stabilities of pRNA self-assembly in M2, GA1, and ϕ29 sequences are within experimental error. The trimer dissociation constant for SF5 (1.88×10^{-15} M^2) is similar to the trimer dissociation constant for ϕ29 (8.58×10^{-14} M^2) previously measured by equilibrium sedimentation (44). Thus, similar stabilities of tertiary and quaternary interactions occur in pRNA assembly of different natural sequences.

Any Combination of Consecutive Watson-Crick or GU Pairs Facilitates pRNA Dimer Formation—To test the potential of the interlocking loops to direct pRNA self-assembly, several mutations swapping the interlocking loop sequences were studied (Fig. 4 and Table 3). Surprisingly, all interlocking loop sequences with at least two consecutive Watson-Crick or GU pairs formed dimers. In the absence of magnesium, no dimer was formed, which is consistent with previous studies of the magnesium dependence of ϕ29 dimerization (38, 39). The overall architecture in pRNA may be conducive to forming dimers and place the loops in the correct position to interact, and then the pairing interactions between the loops may simply stabilize the dimer.

All of the mutants except mutant 1 could form Watson-Crick or GU pairs. For example, mutant 3 has 5′-UU-3′ and 5′-AA-3′ in the CE and D loops, respectively; and mutant 6 has 5′-AU-3′ and 3′-UA-5′ in the CE and D loops, respectively. Mutant 2

TABLE 2
Dissociation constants and free energy of pRNA multimer formation at 4 °C

pRNA	Ion condition $[Mg^{2+}]$	Ion condition $[Na^+]$	K_d	$-\Delta G^0_4$	Interacting bp	$-\Delta G^{0\,a}_4$	K_d [b]
	mM		M	kcal/mol		kcal/mol	M
ϕ29	10	0	6.45×10^{-7} [c]	7.85	AACC/GGUU	9.11	6.54×10^{-8}
					AACC/GGUU	4.33[f]	3.85×10^{-4} [f]
M2	10	0	9.30×10^{-7}	7.65	AUC/GAU	5.41	5.41×10^{-5}
	10	5	1.11×10^{-6} [c]	7.55			
GA1	10	0	1.52×10^{-6}	7.37	CA/UG	2.98	4.47×10^{-3}
	10	5	2.73×10^{-6} [c]	7.06			
SF5	10	5	5.67×10^{-7} [d]	7.92 [d]	AAA/UUU	3.11	3.53×10^{-3}
			1.88×10^{-1} [c,e]	18.67 [e]			

[a] Free energy of Watson-Crick base pairing was calculated with nearest neighbor parameters (45).
[b] The predicted dissociation constant of dimer formation was calculated from the predicted ΔG^0_4 for the Watson-Crick interacting base pairs.
[c] The reported dissociation constants are the average of at least three measurements with an estimated error of ±15%.
[d] The K_d for dimer formation was calculated assuming that dimer and trimer formation in SF5 pRNA follows two independent pathways.
[e] The value is the K_d for trimer formation.
[f] The free energy for the ϕ29 base pairing considers the two GC base pairs, consistent with the NMR data of this interaction (21).

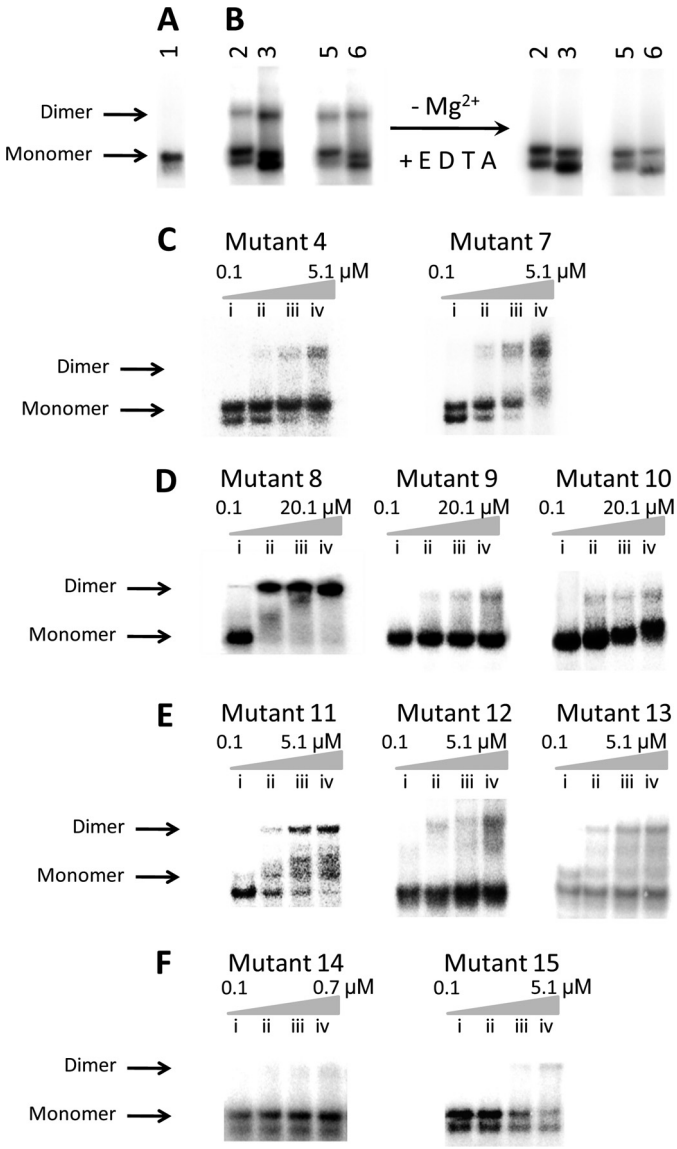

FIGURE 4. **Native gel analysis of pRNA mutants.** The pRNA samples were renatured from 90 to 4 °C by snap cooling on ice in 5 mM NaCl and 10 mM $MgCl_2$ with 90 mM Tris and 200 mM boric acid (pH 7.5), but there was no $MgCl_2$ in the RNA samples or gels in the *right panel* in *B*. *A*, 20 μM mutant 1 pRNA formed only a monomer. *B*, 0.1 μM mutants 2–5 formed dimers in the presence of $MgCl_2$ but formed only monomers in the absence of $MgCl_2$. *C*, concentration dependence of dimer formation for mutants 4 and 7. The pRNA concentrations in *lanes i–iv* are 0.1, 0.3, 1.1, and 5.1 μM, respectively. *D*, concentration dependence of dimer formation for mutants 8–10. The pRNA concentrations in *lanes i–iv* are 0.1, 2.6, 7.6, and 20.1 μM, respectively. *E*, concentration dependence of dimer formation for mutants 11–13. The pRNA concentrations in *lanes i–iv* are 0.1, 0.3, 1.1, and 5.1 μM, respectively. *F*, concentration dependence of dimer formation for mutants 14 and 15. The pRNA concentrations for mutant 14 in *lanes i–iv* are 0.1, 0.2, 0.3, and 0.7 μM, respectively, and those for mutant 15 are 0.1, 0.3, 1.1, and 5.1 μM, respectively. The same amount of labeled ^{32}P was added to all samples, and the amount of monomer and dimer was calculated as a ratio of the measured intensities in monomer and dimer bands.

could form only GU pairs between the loops. However, consecutive terminal GU pairs can stabilize RNA helices, and helices with only GU pairs can form (46). Mutant 5 could form a mixture of Watson-Crick and GU pairs, 5′-AUC-3′ and 3′-UGG-5′ in the CE and D loops, respectively. Some mutated pRNA sequences had two lower bands, suggesting that the monomer may fold into more than one conformation. However, at least one of these conformations was able to form dimers. Secondary structure predictions from RNAstructure 4.6 (39) for all of the ϕ29 mutants suggested that all of the sequences can fold into similar monomer secondary structures as wild-type ϕ29. The combinations of mutants 2 and 3 and mutants 5 and 6 have the potential to form heterodimers, although the heterodimer and homodimers could not be distinguished on a gel (supplemental Fig. S5).

The only sequence that did not form dimers under any conditions is mutant 1, with only U nucleotides in the loop. The molecular weight of mutant 1 was confirmed by analytical ultracentrifugation (Table 1). The inability of mutant 1 to form a dimer even at 20 μM suggests that the renaturing process does not cause the monomers to completely unfold all helices and then refold as one long duplex with internal loops but rather supports the interpretation that dimers are forming between two folded monomers. The wide variation in dissociation constants in the mutants is also inconsistent with the possibility of forming one long duplex. The 3 orders of magnitude range of dissociation constants for the mutants is much greater than would be expected for internal loop sequence variation in a long duplex (47, 48). Chemical modification experiments show many changes upon dimerization but do not conclusively prove monomer or dimer formation (49). The snap cooling procedure and the formation of trimers and higher order multimers also support the interpretation of self-assembly among folded monomers.

Mutants 14 and 15 form a small amount of dimer with increasing concentration (Fig. 4*F*). Previous studies of these pRNA mutants did not detect dimer formation using less sensitive UV absorption detection (5, 7, 9). The increased sensitivity of ^{32}P-labeled RNA enables detection of dimer formation at 2 orders of magnitude lower concentration than the wild-type sequence. These mutants have the potential to form AU and GU pairs in the interlocking loops. The formation of base pairs in the interlocking loops in mutants 14 and 15 is consistent with the low levels of packaging activity retained by these mutants (5).

Sequence Variation outside the Interlocking Loops Contributes to the Stability of pRNA Self-assembly—The predicted free energies of Watson-Crick pairing between the interlocking loops does not fully account for the stabilities of pRNA self-assembly in natural sequences (Table 2). The assembly of the mutant pRNA sequences suggests that the pairing in the loop-loop interaction stabilizes the intrinsic propensity of the pRNA molecule's overall shape and architecture to dimerize. Within the context of the ϕ29 pRNA architecture or surrounding sequence, the CE and D loop sequences for SF5, M2, and GA1 were studied as single and double mutants. For example, mutants 2–4 contain the SF5 sequence in the CE loop, D loop, or both loops, respectively, in the ϕ29 pRNA architecture (Fig. 4 and Table 3). Similarly, mutants 5–7 and mutants 8–10 contain the M2 and GA1 loop sequences in the context of the ϕ29 pRNA architecture. In addition, the ϕ29 CE and D loop sequences were studied in the context of the SF5, M2, and GA1 surrounding sequences (mutants 11–13).

For the SF5 loop sequences in the ϕ29 surrounding sequences, changing either the CE or D loop (mutant 2 or 3) did

TABLE 3
pRNA CE and D loop mutants

Mutant	Surrounding sequence	Loop		Loop sequence		Estimated K_d[a]	Estimated $-\Delta G_4^{0}$[b]
		CE bulge loop	D hairpin loop	CE bulge loop	D hairpin loop		
						M	kcal/mol
1	ϕ29			GUUUUUUU	UUUUU	[c]	
2	ϕ29	SF5	ϕ29	GUUGUUUU	UGGUU	1.10×10^{-6}	7.56
3	ϕ29	ϕ29	SF5	GAUUAAACC	AAA	6.50×10^{-7}	7.85
4	ϕ29	SF5	SF5	GUUGUUUU	AAA	2.76×10^{-5}	5.78
5	ϕ29	M2	ϕ29	GUAUAUC	UGGUU	6.21×10^{-7}	7.87
6	ϕ29	ϕ29	M2	GAUUAAACC	GAU	6.85×10^{-7}	7.82
7	ϕ29	M2	M2	GUAUAUC	GAU	1.26×10^{-5}	6.21
8	ϕ29	GA1	ϕ29	GCAUCC	UGGUU	[d]	
9	ϕ29	ϕ29	GA1	GAUUAAACC	GUG	2.10×10^{-4}	4.66
10	ϕ29	GA1	GA1	GCAUCC	GUG	1.97×10^{-4}	4.70
11	SF5	ϕ29	ϕ29	GAUUAAACC	UGGUU	[d]	
12	M2	ϕ29	ϕ29	GAUUAAACC	UGGUU	9.73×10^{-6}	6.36
13	GA1	ϕ29	ϕ29	GAUUAAACC	UGGUU	3.12×10^{-5}	5.71
14[e]	ϕ29		ϕ29	GAUUAGCGA	UGGUU	9.73×10^{-5}	5.09
15[e]	ϕ29	ϕ29		GAUUAAACC	UUCGC	3.18×10^{-5}	5.70

[a] Dissociation constants were estimated at the concentrations of mutant pRNA in gels shown in Fig. 4 in the ionic condition of 10 mM Mg^{2+} and 5 mM Na^{+}.
[b] The estimated free energy was calculated with the dissociation constants.
[c] No dimer was formed.
[d] The pRNA formed intermediates between monomer and dimer.
[e] The four consecutive bases (AACC) in CE loop for intermolecular interaction were mutated to GCGA, and those in D loop (GGUU) were mutated to UCGC. Previous experiments studying ϕ29 pRNA dimerization with UV absorbance did not detect any dimerization with these mutants (7). More sensitive ^{32}P labeling detected dimerization of these mutants in the conditions reported under "Experimental Procedures" and for Fig. 4*F*.

not significantly decrease the stability of dimerization compared with wild-type ϕ29. Changing both the CE and D loops to the SF5 sequences (mutant 4) decreased the dimerization stability by 2 orders of magnitude, however. Similarly, the single M2 loop mutation 5 and 6 had little effect, whereas the double M2 loop mutation 7 decreased dimerization stability by over an order of magnitude. In the case of the GA1 loop sequence mutants in the ϕ29 architecture (mutants 8–10), the measureable single mutant 9 and the double mutant 10 decreased the stability of dimerization by 2 orders of magnitude relative to wild-type ϕ29. Thus, changing both the CE and D loops together does not recover stability by providing the matching interlocking loop sequence but rather further decreases stability in a context-dependent manner.

All of the double CE-D loop mutants (mutants 4, 7, and 10) were not only less stable dimers than wild-type ϕ29 but also less stable than any of the natural wild-type pRNA sequences (Tables 2 and 3). For example, mutant 10 with the GA1 interlocking loop sequences in the context of the ϕ29 architecture has a K_d of 1.97×10^{-4} M; the dimerization dissociation constant for mutant 10 is 2 orders of magnitude less favorable than the natural GA1 pRNA sequence ($K_d = 2.73 \times 10^{-6}$ M). Thus, additional tertiary and quaternary interactions outside of the loop-loop interaction are likely responsible for the 2 orders of magnitude difference in dimerization between these double mutants and the natural pRNA sequences.

The contributions to dimer stability of the loop sequences and the surrounding sequences are interdependent and not simply additive. For example, the GA1 surrounding architecture may provide very stabilizing interactions for the GA1 CE and D interlocking loops because ϕ29 and GA1 pRNAs have similar stabilities in dimer formation, but mutant 10 dimerization (GA1 loop sequences and the ϕ29 surrounding sequence) is much less favorable. One prediction from these observations could be that the combination of ϕ29 loop sequences in the GA1 surrounding architecture (mutant 13) would be exceptionally stable. However, both mutant 10 (GA1 loop sequences in the ϕ29 surrounding sequence) and mutant 13 (ϕ29 loop sequences in GA1 surrounding sequences) formed less stable dimers than either natural ϕ29 or GA1 pRNA. Thus, the contributions of the loop sequences and the surrounding architecture are synergistic in pRNA dimer formation.

When the ϕ29 CE and D loop sequences were inserted into the surrounding sequences of SF5, M2, and GA1 (mutants 11–13), the stability of dimer formation was reduced by 1–2 orders of magnitude in a dissociation constant. Thus, the decrease in dimer formation stability when mutating the loop sequences is not unique to the ϕ29 architecture. Interestingly, mutant 4 with the SF5 CE and D loops in the context of the ϕ29 architecture and mutant 11 with the ϕ29 CE and D loops in the SF5 architecture did not show any propensity for trimer formation or high order multimers.

Thus, the sequence of the interlocking loops and the surrounding sequence together create stable dimers. The surrounding sequences may correctly position the nucleotides to form Watson-Crick or GU pairs. The surrounding sequences may have complementary shapes that facilitate dimer formation but still require stable pairing in the interlocking loops. Forming pairs in the interlocking loops may change the conformation and stability of the surrounding sequence, for example, by stabilizing a particular coaxial stacking arrangement in the multibranch loop that is dynamic in the monomer but more rigid in the dimer. The bulged nucleotides in the surrounding architecture may then further stabilize dimer formation but only when the right combination of pairing interactions and conformational changes occurs during dimerization.

All Natural pRNA Sequences Require Magnesium for Self-assembly—Magnesium often stabilizes RNA tertiary interactions (50) and also stabilizes the quaternary interactions in pRNA assembly. For example, reducing the magnesium concentration increases the ϕ29 pRNA concentration necessary for trimer formation. In the presence of 2 mM $MgCl_2$ and 5 mM NaCl, the ϕ29 pRNA did not form a trimer until 10.1 μM pRNA, whereas trimer formation occurred at 0.64 μM in 10 mM $MgCl_2$

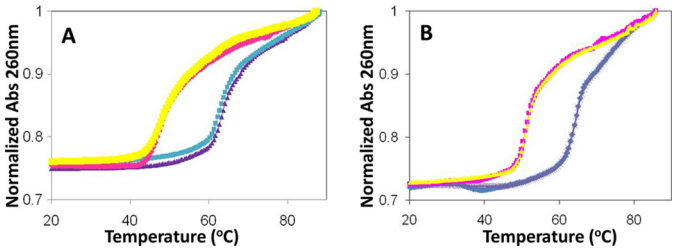

FIGURE 5. **Optical melting curves of ϕ29 (*A*) and GA1 (*B*) pRNAs at 3 μM RNA and 100 mM NaCl (*yellow*); 10 μM RNA and 100 mM NaCl (*pink*); 3 μM RNA, 100 mM NaCl, and 5 mM $MgCl_2$ (*blue*); and 10 μM RNA, 100 mM NaCl, and 5 mM $MgCl_2$ (*purple*).** *Abs*, absorbance.

and 5 mM NaCl (supplemental Fig. S6). None of the natural pRNA sequences formed dimers without magnesium in up to 100 mM NaCl, which suggests that higher monovalent ionic conditions do not compensate for magnesium.

Fig. 5 shows the effects of adding magnesium on the thermal stability of ϕ29 and GA1 pRNAs. The thermal unfolding of pRNA is highly cooperative as indicated by the sharp transition in UV absorbance. The temperature at which this transition occurred did not change with increasing concentration of RNA from 3 to 10 μM, which is consistent with unimolecular unfolding. No transition was observed below 20 °C. In ϕ29 and GA1 sequences, both the monomer and dimer formed at 4 °C in the optical melting buffer conditions of 100 mM NaCl and 10 mM $MgCl_2$ (supplemental Fig. S7). If there is any hyperchromicity associated with the loss of intermolecular base pairs, then this transition occurs together with the unfolding of the pRNA molecule. In the absence of magnesium, the ϕ29 and GA1 pRNAs showed similar melting temperatures. The addition of 5 mM $MgCl_2$ significantly stabilized ϕ29 and GA1 pRNAs and increased the melting temperatures from 49.6 to 63.5 °C and from 50.2 to 63.9 °C, respectively. Further increases in $MgCl_2$ to 10 mM provided no additional stability (supplemental Fig. S7), which indicates a specific ion effect rather than a general increase in stability from increased salt concentration.

The CD spectra are consistent with the addition of magnesium stabilizing a transition from one folded conformation to another folded conformation rather than inducing a transition from unfolded to folded conformations. The CD spectra of ϕ29 and GA1 pRNAs in different ionic conditions showed a maximum peak near 260 nm, a minimum peak near 210 nm, and a small negative peak near 290 nm (supplemental Fig. S8), which are characteristic of A-form RNA helices. The addition of 10 mM $MgCl_2$ reduced slightly the maximum peak at 260 nm, which also suggests a specific ion effect.

Sodium Ion Concentrations and Temperature Affect pRNA Assembly Differently for Different Natural Sequences—Sodium ions and renaturing temperature synergistically affected pRNA self-assembly. For example, at room temperature in the presence of 10 mM $MgCl_2$ (supplemental Fig. S9, *lane 3* of each pRNA), ϕ29 pRNA formed monomers and dimers; M2 pRNA formed dimers and a multimer; GA1 pRNA formed almost only monomer; and SF5 pRNA formed many higher order multimers. SF5 pRNA showed extraordinary competence of multimerization at room temperature but no self-assembly with snap cooling to 4 °C in 10 mM $MgCl_2$ and 100 mM NaCl (supplemental Fig. S10). In contrast, SF5 formed a monomer and trimer with snap cooling to 4 °C in lower sodium chloride concentrations, *i.e.* 10 mM $MgCl_2$ and 5 mM NaCl (Fig. 3). The complex sequence-dependent effects of sodium ion concentration and renaturation temperature may result from the differences in the architectures of different pRNA natural sequences. The different multibranch loops and bulge loops in different pRNA sequences may have different interactions with metal ions or different probabilities for orientations of the helices that could affect pRNA self-assembly.

In conclusion, the four natural pRNA sequences contain very few conserved nucleotides (Fig. 1). The single nucleotide bulges vary in sequence and position in the helix, and the multibranch loops between the A, C, and D helices also vary in size and sequence. Thus, each pRNA sequence offers different opportunities for additional stabilizing tertiary and quaternary interactions. This sequence variation may explain the difference in stabilities between the natural pRNA sequences and the double mutants with the interlocking loop sequences transplanted into different surrounding sequences, differing propensities for multimer formation, and different magnesium ion dependences in different pRNA sequences. Interestingly, the free energy of pRNA dimerization is approximately the same for all pRNA sequences despite different predicted stabilities for the Watson-Crick base pairing interactions in the interlocking loops. Thus, perhaps the pRNA sequences evolved to maintain a minimum stability in multimerization, and as the CE and D loop sequences evolved, the single nucleotide bulges and multibranch loop sequences also evolved to make energetically compensating changes. Thus, pRNA self-assembly may be stabilized by many noncovalent tertiary and quaternary interactions and magnesium ion interactions in addition to the base pairing in the interlocking loops.

Acknowledgments—We thank Dr. Shelley Grimes for the M2 and GA1 genomic DNAs, Dr. Nicola Stonehouse for the plasmid containing the ϕ29 sequence, Dr. Marc Dreyfus (CNRS) for the T7 polymerase mutant, Dr. Haiqing Yu (University of Arizona) for CD data collection, and Becky Myers for T7 preparation in the Schroeder laboratory.

REFERENCES

1. Guo, P. X., Erickson, S., and Anderson, D. (1987) *Science* **236,** 690–694
2. Grimes, S., and Anderson, D. L. (1990) *J. Mol. Biol.* **251,** 559–566
3. Bailey, S., Wichitwechkarn, J., Johnson, D., Reilly, B. E., Anderson, D. L., and Bodley, J. W. (1990) *J. Biol. Chem.* **265,** 22365–22370
4. Zhao, W., Morais, M. C., Anderson, D. L., Jardine, P. J., and Grimes, S. (2008) *J. Mol. Biol.* **383,** 520–528
5. Reid, R., Zhang, F., Benson, S., and Anderson, D. (1994) *J. Biol. Chem.* **269,** 18656–18661
6. Reid, R. J., Bodley, J. W., and Anderson, D. (1994) *J. Biol. Chem.* **269,** 9084–9089
7. Reid, R. J., Bodley, J. W., and Anderson, D. (1994) *J. Biol. Chem.* **269,** 5157–5162
8. Zhang, C., Tellinghuisen, T., and Guo, P. (1997) *RNA* **3,** 315–323
9. Chen, C., Zhang, C., and Guo, P. (1999) *RNA* **5,** 805–818
10. Garver, K., and Guo, P. (1997) *RNA* **3,** 1068–1079
11. Yu, J., Moffitt, J., Hetherington, C. L., Bustamante, C., and Oster, G. (2010) *J. Mol. Biol.* **400,** 186–203
12. Morais, M. C., Koti, J. S., Bowman, V. D., Reyes-Aldrete, E., Anderson, D. L., and Rossmann, M. G. (2008) *Structure* **16,** 1267–1274
13. Xiao, F., Zhang, H., and Guo, P. (2008) *Nucleic Acids Res.* **36,** 6620–6632

14. Guo, P., Zhang, C., Chen, C., Garver, K., and Trottier, M. (1998) *Mol. Cell* **2,** 149–155
15. Zhang, F., Lemieux, S., Wu, X., St-Arnaud, D., McMurray, C. T., Major, F., and Anderson, D. (1998) *Mol. Cell* **2,** 141–147
16. Moffitt, J. R., Chemla, Y. R., Aathavan, K., Grimes, S., Jardine, P. J., Anderson, D. L., and Bustamante, C. (2009) *Nature* **457,** 446–450
17. Smith, D. E., Tans, S. J., Smith, S. B., Grimes, S., Anderson, D. L., and Bustamante, C. (2001) *Nature* **413,** 748–752
18. Chemla, Y. R., Aathavan, K., Michaelis, J., Grimes, S., Jardine, P. J., Anderson, D. L., and Bustamante, C. (2005) *Cell* **122,** 683–692
19. Rickgauer, J. P., Fuller, D. N., Grimes, S., Jardine, P. J., Anderson, D. L., and Smith, D. E. (2008) *Biophys. J.* **94,** 159–167
20. Fang, Y., Cai, Q., and Qin, P. Z. (2005) *Biochemistry* **44,** 9348–9358
21. Kitamura, A., Jardine, P. J., Anderson, D. L., Grimes, S., and Matsuo, H. (2008) *Nucleic Acids Res.* **36,** 839–848
22. Lee, T. J., Schwartz, C., and Guo, P. (2010) *Ann. Biomed. Eng.* **37,** 2064–2081
23. Guo, P. (2005) *J. Nanosci. Nanotechnol.* **5,** 1964–1982
24. Guo, S., Tschammer, N., Mohammed, S., and Guo, P. (2005) *Human Gene Ther.* **16,** 1097–1109
25. Shu, D., Huang, L. P., Hoeprich, S., and Guo, P. (2003) *J. Nanosci. Nanotechnol.* **3,** 295–302
26. Guo, S., Huang, F., and Guo, P. (2006) *Gene Ther.* **13,** 814–820
27. Ko, S. H., Chen, Y., Shu, D., Guo, P., and Mao, C. (2008) *J. Am. Chem. Soc.* **130,** 17684–17687
28. Liu, H., Guo, S., Roll, R., Li, J., Diao, Z., Shao, N., Riley, M. R., Cole, A. M., Robinson, J. P., Snead, N. M., Shen, G., and Guo, P. (2007) *Cancer Biol. Ther.* **6,** 697–704
29. Zhang, H. M., Su, Y., Guo, S., Yuan, J., Lim, T., Liu, J., Guo, P., and Yang, D. (2009) *Antiviral Res.* **83,** 307–316
30. Severcan, I., Geary, C., Verzemnieks, E., Chworos, A., and Jaeger, L. (2009) *Nano Lett.* **9,** 1270–1277
31. Chworos, A., Severcan, I., Koyfman, A. Y., Weinkam, P., Oroudjev, E., Hansma, H. G., and Jaeger, L. (2004) *Science* **306,** 2068–2072
32. Afonin, K. A., Bindewald, E., Yaghoubian A. J., Voss, N., Jacovetty, E., Shapiro, B. A., and Jaeger, L. (2010) *Nat. Nanotechnol.* **5,** 676–682
33. Severcan, I., Geary, C., Chworos, A., Voss, N., Jacovetty, E., and Jaeger, L. (2010) *Nat. Chem.* **2,** 772–779
34. Grabow, W. W., Zakrevsky, P., Afonin, K. A., Chworos, A., Shapiro, B. A., and Jaeger, L. (2011) *Nano Lett.* **11,** 878–887
35. Nasalean, L., Baudrey, S., Leontis, N. B., and Jaeger, L. (2006) *Nucleic Acids Res.* **34,** 1381–1392
36. Afonin, K. A., Cieply, D. J., and Leontis, N. B. (2008) *J. Am. Chem. Soc.* **130,** 93–102
37. Koyfman, A. Y., Braun, G., Magonov, S., Chworos, A., Reich, N. O., and Jaeger, L. (2005) *J. Am. Chem. Soc.* **127,** 11886–11887
38. Chen, C., and Guo, P. (1997) *J. Virol.* **71,** 495–500
39. Fuller, D. N., Rickgauer, J. P., Jardine, P. J., Grimes, S., Anderson, D. L., and Smith, D. E. (2007) *Proc. Natl. Acad. Sci. U.S.A.* **104,** 11245–11250
40. Atz, R., Ma, S., Gao, J., Anderson, D. L., and Grimes, S. (2007) *J. Mol. Biol.* **369,** 239–248
41. Guillerez, J., Lopez, P. J., Proux, F., Launay, H., and Dreyfus, M. (2005) *Proc. Natl. Acad. Sci. U.S.A.* **102,** 5958–5963
42. Demeler, B., and van Holde, K. E. (2004) *Anal. Biochem.* **335,** 279–288
43. Brookes, E., and Demeler, B. (2006) *Prog. Colloid Polymer Sci.* **131,** 32–38
44. Robinson, M. A., Wood, J. P., Capaldi, S. A., Baron, A. J., Gell, C., Smith, D. A., and Stonehouse, N. J. (2006) *Nucleic Acids Res.* **34,** 2698–2709
45. Xia, T., SantaLucia, J., Jr., Burkard, M. E., Kierzek, R., Schroeder, S. J., Jiao, X., Cox, C., and Turner, D. H. (1998) *Biochemistry* **37,** 14719–14735
46. Nguyen, M. T., and Schroeder, S. J. (2010) *Biochemistry* **49,** 10574–10581
47. Mathews, D. H., Disney, M. D., Childs, J. L., Schroeder, S. J., Zuker, M., and Turner, D. H. (2004) *Proc. Natl. Acad. Sci. U.S.A.* **101,** 7287–7292
48. Turner, D. H., and Mathews, D. H. (2010) *Nucleic Acids Res.* **38,** D280–D282
49. Trottier, M., Mat-Arip, Y., Zhang, C., Chen, C., Sheng, S., Shao, Z., and Guo, P. (2000) *RNA* **6,** 1257–1266
50. Cate, J. H., Gooding, A. R., Podell, E., Zhou, K., Golden, B. L., Kundrot, C. E., Cech, T. R., and Doudna, J. A. (1996) *Science* **273,** 1678–1685
51. Borer, P. N. (1975) in *Handbook of Biochemistry and Molecular Biology: Nucleic Acids* (Fasman, C. D., ed) Vol. 1, 3rd Ed., p. 589, CRC Press, Cleveland, OH